CONTRIBUTION TO THE UNDERSTANDING OF THE MICROSTRUCTURE OF FIRST GENERATION SI-C-O FIBERS

Francis Teyssandier, Géraldine Puyoo, Stéphane Mazerat, Georges Chollon, René Pailler, Florence Babonneau[1]
Laboratoire des composites thermostructuraux, Université de Bordeaux 1, Pessac, France.
1 Chimie de la Matière Condensée de Paris, Collège de France, Paris, France.

ABSTRACT:

As compared to the most recent SiC-based ceramic fibers, first generation fibers include a significant amount of oxygen and free carbon. Though a large number of papers have been devoted to understanding the microstructure of these fibers, their composition and microstructure are still controversial. This communication is intended to propose a microstructure description of these fibers according to their composition in the Si-C-O isothermal section of the phase diagram. The proposed microstructure is deduced from a large set of characterizations including XRD, Raman spectroscopy, RMN, and elemental analysis. Three Nicalon and four Tyranno fibers are thus characterized. Their fracture behavior is also described.

KEYWORDS: Si-C-O fibers, Fiber composition, Fiber microstructure.

INTRODUCTION

Ceramic matrix composites (CMC) were first developed for applications in severe environments: at high temperature, under mechanical stress, in oxidative environments and even under radiations. Such demanding applications require very high properties that are obtained by use of high performance materials. New trends are to develop CMC materials for very long life time applications but at lower temperatures and with a reduced stress level. Such CMC that are aimed at being used in civil aeronautics (aircraft engine plug or exhaust…), do not require the most capable third generation fibers. Instead, the less demanding parts in terms of performance can be designed with less expensive fibers of the first generation. The aim of the present paper is to compare the properties of a variety of first generation silicon carbide fibers.

Since the pioneering work of Yajima et al.[1] in the seventies, the SiC fibers have been improved in order to increase the creep and oxidation resistance[2]. Three families of SiC fibers have been successively developed from the first generation that included carbon and oxygen in excess, to the third generation, which is composed of almost pure silicon carbide. The durability of SiC/SiC composites is at last related to the fibers lifetime, i.e., their sensitivity to oxidation or subcritical crack growth. This latter mechanism is largely influenced by the composition and the structure of the Si-O-C fibers and is expected to be accelerated by the presence of free carbon. The percentage of oxygen and the SiC grain size may also have a significant influence on the fiber reactivity. We therefore undertook the characterization of a wide variety of first generation silicon carbide fibers in order to provide a detailed description of their microstructure and properties.

The microstructure of first generation SiC fibers is globally known. It can be described as a continuum consisting of glassy silicon oxycarbide binding pure β-SiC nanocrystals and including free carbon nanodomains called basic structural units (BSU)[3-8].

Many authors have contributed to the assessment of the microstructure of the various phases composing the Si-O-C fibers. In 1989, Laffon et al.[3] studied the NicalonTM NG100 and NG200 fibers mainly by EXAFS and X-ray diffraction and proposed a model of structure including a continuum of β-SiC nanocrystals embedded in a Si-C-O glass consisting of mixed SiO_XC_Y (X+Y=4) tetrahedral environments. Carbon BSU are described as aggregates composed of graphene layers with edges saturated with hydrogen, i.e. without any chemical bonding with the Si-O-C continuum. In 1993, Le

Coustumer et al.[5] studied the Nicalon fiber NLM202. They determined the following composition: 55wt% of β-SiC crystals, 40wt% of amorphous $SiO_{1.15}C_{0.85}$ and 5wt% of free carbon. Knowing the percentage of free carbon and the atomic chemical composition, they calculated the proportion of each phase. An average grain size of 1.6nm was measured using (111)-SiC Dark Field transmission imaging (DF-TEM).

In 1996 Bodet et al.[9] calculated phase proportions and composition of the fiber Nicalon NLP201 knowing atomic chemical composition and SiC/SiO_xC_y ratio as determined by XPS analysis (from the various Si2p peak components). An average β-SiC grain size of 2.7 nm was measured using (111)-SiC DF-TEM image.

More recently, by use of density functional theory, P. Kroll calculated the structure and properties of amorphous silicon oxycarbide glasses, pure[10] or including a free carbon phase[11].

RESULTS AND DISCUSSION

We studied the following first generation SiC fibers: Nicalon NLM202 and 207 from Nippon Carbon, and Tyranno S, ZMI, LoxM from UBE. We also studied the Tyranno AM and Nicalon NLP101 which are not currently commercialized. Their composition and structure are nevertheless interesting to compare to other fibers.

The atomic composition of the whole fiber was first determined by chemical analysis. We then successively studied the β-SiC nanocrystallites by both X-ray diffraction (XRD) and high resolution transmission electron microscopy (HRTEM). The pure Si-C-O glass phase has the composition $SiC_xO_{2(1-x)}$. Its composition was both deduced from the atomic composition and by nuclear magnetic resonance (NMR) ^{29}Si analysis. The amount of free carbon was both deduced from the difference between the atomic composition of the fiber and the composition of the Si-C-O continuum, as well as from ^{13}C-NMR analysis. We also characterized the in-plane disorder of carbon BSU by Raman spectroscopy.

Elemental Composition of Fibers

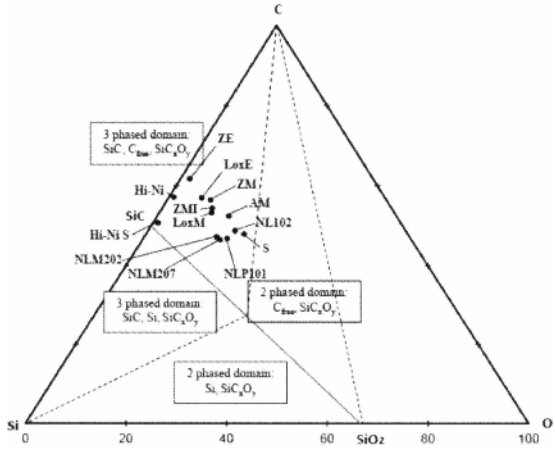

Figure 1: composition of first generation SiC fibers presented in the ternary section of the Si-O-C phase diagram.

The elemental composition of fibers was measured by chemical analysis at the CNRS facility in Solaize. The content of silicon, as well as of Zr, Ti and Al (that are present in limited amounts), was determined by Inductively Coupled Plasma - Atomic Emission Spectroscopy. The carbon concentration was deduced from the amount of CO_2 resulting from oxidation. The oxygen concentration of fibers was deduced from the amount of carbon monoxide formed by reaction at high temperature between ground fibers and the carbon crucible in which they are disposed. Hydrogen was deduced from the amount of water vapor formed by oxidation. The compositions of the fibers are plotted in the isothermal Si-C-O ternary section in figure 1. The Tyranno S fiber has the highest oxygen content and also the largest amount of amorphous $SiC_xO_{2(1-x)}$ phase.

Phase Composition of the Fibers: Assumptions

The pure Si-C-O amorphous phase which is composed of mixed tetrahedral environments SiO_XC_Y (X+Y=4) can be described using a rule of mixture between silica and silicon carbide similar to: $SiC_xO_{2(1-x)}$= x SiC + (1-x) SiO_2. We assumed that the so called "free carbon" phase, embedded into the continuum is not bonded to the amorphous $SiC_xO_{2(1-x)}$ glass nor the β-SiC grains[7]. We could thus infer that all the oxygen atoms are bonded to silicon, the remaining silicon being bonded to carbon. Carbon atoms that are not bonded to sp^3-silicon are hence part of the free carbon domains (sp^2-C).

Composition of the Si-C-O Continuum

Composition of the Si-C-O continuum (β-SiC + amorphous silicon oxycarbide) was deduced from the atomic composition measured by chemical analysis on each type of fiber. It was calculated according to the formula $SiC_xO_{2(1-x)}$ on grounds of assumptions described in the preceding paragraph.

The composition was also measured by nuclear magnetic resonance (NMR) analysis of silicon (^{29}Si) carried out on grounded fibers. NMR analysis enabled us to characterize quantitatively the proportion of the various allowed tetrahedral environments of silicon: $\underline{Si}C_4$, $\underline{Si}C_3O$, $\underline{Si}C_2O_2$, $\underline{Si}CO_3$ and $\underline{Si}O_4$. The recorded spectra were decomposed into five peaks, one for each silicon environment, the amount of each environment being proportional to the surface of the corresponding peak. The related chemical shifts are observed in the following order: $\delta(\underline{Si}C_3O) > \delta(\underline{Si}C_4) > \delta(\underline{Si}C_2O_2) > \delta(\underline{Si}O_3C) > \delta(\underline{Si}O_4)$. It is interesting to notice that the chemical shift of the $\underline{Si}C_3O$ environment is not, as expected, located between those of SiC_4 and SiC_2O_2, due to a non-linear dependence of the chemical shift (δ) to the charge (q) of atoms.

Compositions obtained by both approaches are in good accordance (figure 2). This result validates our assumptions and especially the absence of bonding between BSU and their neighboring phases.

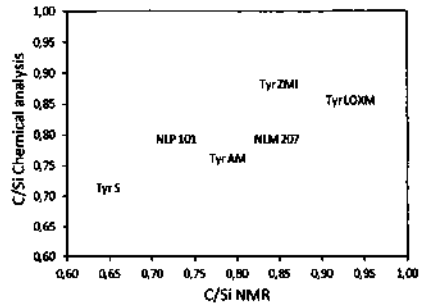

Figure 2: C/Si ratio in the Si-C-O continuum of the various fibers: comparison between calculations based on atomic composition and NMR measurements

NMR measurements revealed that both Nicalon NLP101 and NLM207, as well as Tyranno S and AM include a significant amount of SiO_4 environments (11% for Tyranno S and Nicalon NLP101). This observation provides evidence of a bulk silicon oxycarbide phase between the β-SiC grains and the BSU.

SiC Characterization by X-Ray Diffraction

The amount of crystallized β-SiC phase included in each fiber was determined by X-ray diffraction, carried out on grounded fibers, and including an internal silicon standard. The quantitative analysis was performed by comparing the areas of SiC and Si peaks after calibration with a known mixture. The error of such a procedure was estimated at 4 wt%.

The mean size of SiC crystallites was assessed by the Scherrer formula. As the basic formula assumes monodisperse spherical particles, we used a modified formula including a corrective factor[12,13] to account for the real crystals:

$$L = \frac{k\lambda}{D\cos\theta} \qquad (1)$$

L is the full-width half-maximum (FWHM) of the SiC peak, λ=0.15406 nm Cu-Kα wavelength, k a constant determined to be 0.9 by comparison with crystallite size as observed by TEM and D the mean size of the SiC crystallites.

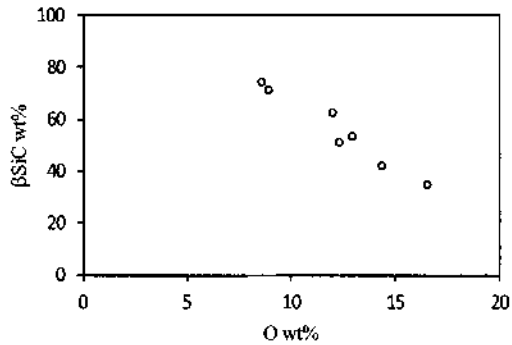

Figure 3: β-SiC crystallite size as a function of the oxygen wt%

The amount of β-SiC crystallites is clearly correlated to the oxygen content of the fiber: the higher the oxygen content, the less the amount of β-SiC crystallites (figure 3). This behavior is in accordance with the Si-C-O phase diagram. It was furthermore observed that the size of the β-SiC crystallites increases with their amount.

Determination of the Free Carbon Content

The amount of free carbon embedded into the continuum was deduced from the atomic composition of the fiber, according to the above described calculation. It was also measured by NMR ^{13}C analysis. The recorded spectrum is composed of two broad peaks at ~19ppm and 119ppm which respectively correspond to C sp3 and C sp2. From the proportion of each type of carbon hybridization, it is possible to estimate the amount of carbon bonded to silicon and the amount of free carbon.

The amount of free carbon measured by the two approaches are in good accordance (figure 4) and shows the same order among fibers. It can nevertheless be observed that amount of free carbon deduced from the measured atomic composition is always higher than the amount measured by NMR. As a general trend, carbon content of Tyranno fibers is much higher than that of Nicalon fibers, because of the type of polymer used as precursor. The maximum carbon content is measured in the Tyranno S fiber and the minimum in the Nicalon NLM207.

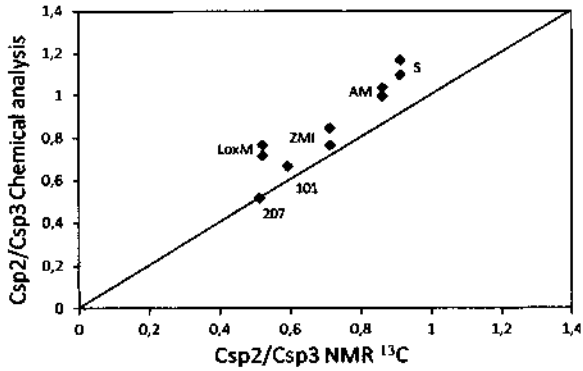

Figure 4: comparison between the ratios between free and tetrahedral carbon deduced from the measured atomic composition of the fibers and its measurement by NMR 13C.

Fractographic Examination of Rupture Patterns

The mechanical properties of fibers are strongly dependent on their chemical composition. For instance, first generation Si-C-O fibers have a tensile modulus of about 200 GPa[6], though the modulus of near stoichiometric fibers reaches almost 300-400 GPa[14]. The morphology of the rupture surface, which is typical of brittles materials, is indicative of the failure mechanism: mirror, mist or hackle-like and crack branching[15-17]. The rupture pattern and its boundaries were used to identify the size of the initial flaw[23-24], assess toughness[18,19], strength[19-22], or residual surface stress[21,24].

Single fiber tensile properties were measured on a micro-tensile testing machine at a constant loading rate of 0.5%.min^{-1} using a gauge length of 25 mm. In order to obtain a good statistical analysis, 40 to 50 samples were tested for each type of fiber. The fiber diameter was measured by laser diffraction prior to testing, and was observed post mortem by SEM.

SEM Observations

SEM observations of fracture surfaces are aimed at identifying the crack origin, measuring the area of typical flaw features and checking the diameter of the fiber. Among the several hundreds of rupture surfaces that were observed by SEM, seven typical families of characteristic flaws were identified: five are originating from surface flaws and two from internal flaws. These characteristic flaws are shown in Figure 5. The A-type flaws have a well-known penny shape contour, the B flaws are small particles present at the surface of the fibers, the C flaws are small surface damages that may result from manipulation or contact between fibers, and the D flaws are chemical composition heterogeneities[17]. In the case of E-type flaws, though rupture clearly originates from the surface, the flaws cannot be observed by SEM because of their particularly small size or the poor image contrast. Concerning the rupture induced by internal flaws, the F flaws are internal inclusions[25] or voids and G

flaws are typical penny shaped cracks (similar to A). These latter flaws were only observed on Hi-Nicalon fibers. A statistical analysis of the flaws responsible for the fiber ruptures is summarized in Figure 6. When plotting, for each fiber, the proportion of ruptures originating from internal and surface flaws, the behavior of the Hi-Nicalon fiber is clearly different from that of the other fibers: almost all their observed ruptures originate from internal flaws. This result is in accordance with G. E. Youngblood et al.[25] observations stating that all of the Hi-Nicalon fiber ruptures originate from internal flaws, though J. Hurst[26] only observed 60% of ruptures induced by internal flaws. As a general trend, the proportion of Nicalon fiber ruptures induced by internal flaws is higher than that of Tyranno fibers, except for the Lox-M fiber.

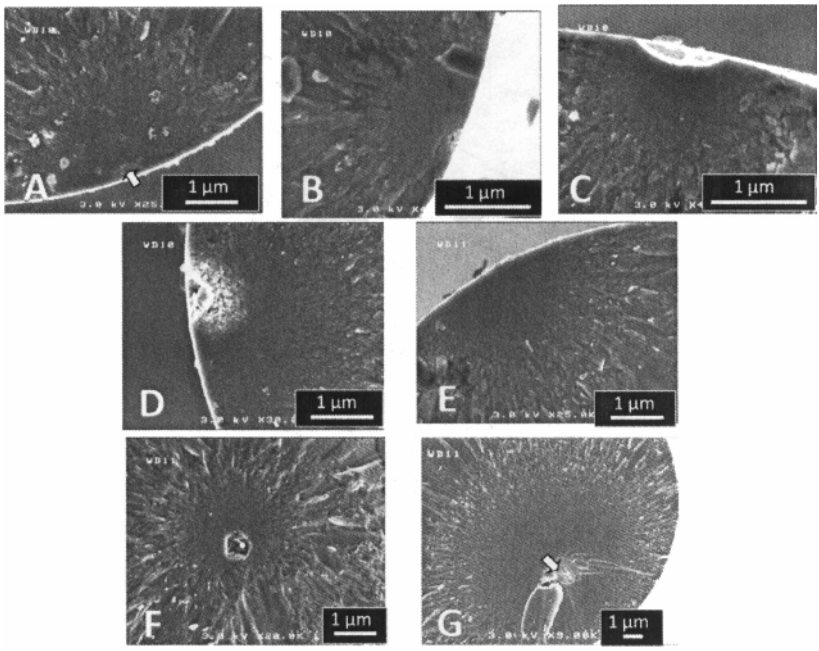

Figure 5: Classification of flaw pattern
Surface flaws: (A) penny shaped crack, (B) particle, (C) surface damage, (D) chemical heterogeneity, (E) no observable trace by SEM,
Internal flaws: (F) internal inclusion, (G) penny shaped crack

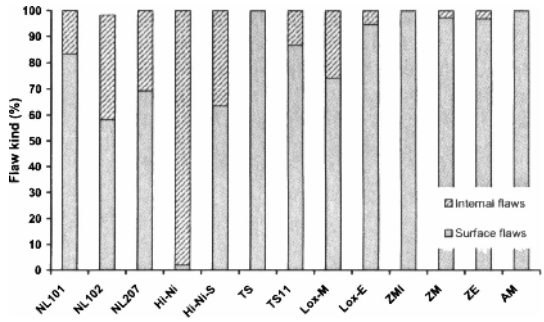

Figure 6: ratio between surface and internal flaws responsible for ruptures for the various fibers

During tensile tests, different stages of crack propagation are usually observed, corresponding to four concentric domains of the fracture pattern[16] (Figure 7). Close to the initial flaw, a smooth mirror region corresponds to an increase of the crack velocity that reaches its maximal value at the edge of this domain. In the mist domain surrounding the mirror domain, the crack dissipates energy by generating micro cracking. As the crack propagates, more energy is available and larger cracks nucleate in a domain referred to as hackle. The final stage corresponds to macroscopic cracks propagating through the entire section of the fiber.

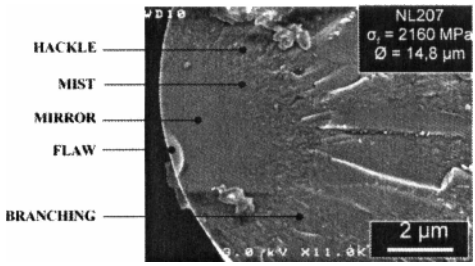

Figure 7: Typical fracture surface pattern and characteristic domains observed on SiC fibers.

Strength and Toughness

From experimental work carried out by many authors on mono or polycrystalline brittle materials, it can be inferred that the strength of the fiber is proportional to the inverse square root of the radius of the mirror domain[16, 27, 28]. Such a relationship was determined for the various fibers and is illustrated in the case of NL207 fiber (figure 8). The experimental points were fitted by a straight line assuming that the residual stress resulting from synthesis can be neglected (straight line drawn through zero). The value of the deduced mirror constant (2.37 $MPa.m^{1/2}$) is close to the Am values reported by L. C. Sawyer (2 $MPa.m^{1/2}$)[17] or A. J. Eckel (2.51 $MPa.m^{1/2}$)[20] on the same fiber.

The same relationship can be established using the radius of hackle or branching domains:

$$\sigma_r = \frac{A_m}{\sqrt{r_m}} \qquad \sigma_r = \frac{A_h}{\sqrt{r_h}} \qquad \sigma_r = \frac{A_b}{\sqrt{r_b}} \tag{2}$$

where A_m, A_h and A_b are constants corresponding respectively to mirror, hackle and branching domains and r_m, r_h and r_b their respective radii.

Though Am is almost exclusively used by the authors, the A_h or A_b constants can provide the same results and are easier to measure by fractographic examination. Indeed, the smaller size of the mirror region and the difficulty to accurately determine its boundary with the mist region are a source of error, which may explain the discrepancies found in literature. We found A_m values ranging from 1.7 to 3.0, A_h in the range 1.9 - 3.6 and A_b in the range 2.5 - 4.7 MPa.m$^{1/2}$. A_m constants are similar to typical values measured on glass materials.

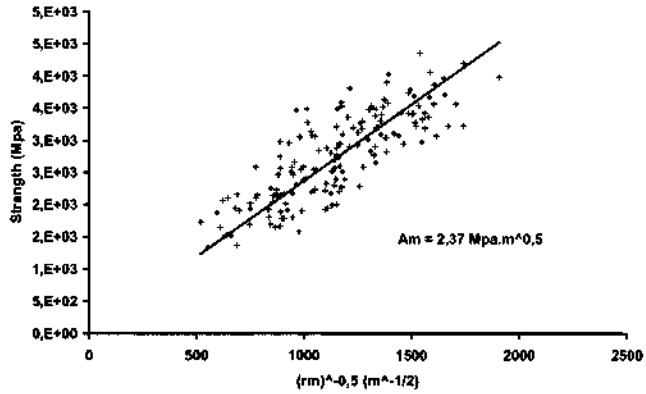

Figure 8: Tensile strength plotted as a function of the inverse square root of the radius of the mirror domain

The fiber fracture behavior depends on its toughness which is quantified by the critical stress intensity factor (K_{IC}). This factor was calculated for all fibers by use of the Griffith equation:

$$K_{IC} = Y\sigma_r\sqrt{a_c} \tag{3}$$

where Y is a geometrical factor (for a penny shaped flaw: $Y = 2/\sqrt{\pi}$), σ_r is the fiber strength and a_c is the flaw size. This calculation was only carried out in the case of penny shaped flaws, the surface of other flaws being difficult to measure. Toughness values of all the SiC fibers of first and second generation, except for Hi-Nicalon, typically range from 1.0 to 1.3. Third generation fibers that are nearly-stoichiometric, have higher toughness but always lower than 2 MPa.m$^{1/2}$.

Combining equations (2) and (3) leads to the definition of a proportional coefficient between the mirror constant and the toughness according to:

$$\frac{2A_m}{\sqrt{\pi}K_{IC}} = \sqrt{\frac{r_m}{a_c}} \tag{4}$$

CONCLUSION

All these characterizations reveal a strong correlation between the microstructure of fibers and their oxygen content. Oxygen is introduced into the fibers during the cross-linking reaction of the polymer precursor. This stage has thus a strong influence on the amount of amorphous Si-C-O formed in the fiber, which is almost proportional to the oxygen content. In particular, the amount and size of β-SiC crystallites are clearly correlated to the oxygen content of the fiber: the higher the oxygen content, the less the amount of β-SiC crystallites, the smaller the β-SiC crystallites. This behavior is in

accordance with the location of the composition of the fibers in the isothermal section of the Si-C-O phase diagram. Both measurements by chemical analysis and NMR of the C/Si ratio in the Si-C-O continuum of the various fibers are in good agreements. This result tends to confirm that the "free carbon" phase, embedded into the continuum is not bonded to the amorphous $SiC_xO_{2(1-x)}$ glass nor the β-SiC grains. The amount of free carbon measured by both chemical analysis and NMR are in good accordance. They show that free carbon content of Tyranno fibers is much higher than that of Nicalon fibers, as the result of the type of polymer used as precursor.

Single fiber tensile properties were measured on a micro-tensile testing machine and their fracture surface observed by SEM. Looking at the proportion of ruptures originating from internal or surface flaws, reveals a clearly different behavior of the Hi-Nicalon fiber as almost all their observed ruptures originate from internal flaws. As a general trend, the proportion of Nicalon fiber ruptures induced by internal flaws is higher than that of Tyranno fiber.

ACKNOWLEDGEMENT
Financial support from the French programme ARCOCE funded by FUI and Aquitaine Region is gratefully acknowledged.

REFERENCES
[1] J. Hayashi, K. Okamura, S. Yajima, Structural analysis in continuous silicon carbide fiber of high tensile strength, *Chemistry Letters*, 1209-12 (1975)
[2] H. Ichikawa, Development of high performance SiC fibers derived from polycarbosilane using electron beam irradiation curing-a review, *J. Ceram. Soc. Jap.*, **114** 455-60 (2006)
[3] C. Laffon, A.M. Flank, P. Lagarde, M. Laridjani, Study of Nicalon-based ceramic fibers and powders by EXAFS spectrometry, X-ray diffractometry and some additional methods, *J. of Mater. Sci.*, **24**, 1503-12 (1989).
[4] L. Porte, A. Sartre, Evidence for a silicon oxycarbide phase in the Nicalon silicon carbide fibre, *J. of Mater. Sci.*, **24**, 271-75 (1989).
[5] P. Le Coustumer, M. Monthioux, A. Oberlin, Understanding Nicalon Fiber, *J. of the Eu. Ceram. Soc.*, **11**, 95-103 (1993).
[6] N. Hochet, M. H. Berger, A. R. Bunsell, Microstructural evolution of the latest generation of small-diameter SiC-based fibers tested at high temperatures, *J. of Microscopy*, **185**, 243-58 (1997).
[7] A.R. Bunsell, A review of the development of three generations of small diameter silicon carbide fibres, *J.Mater.Sci* **41**, 823-39 (2006).
[8] G. Chollon, PhD thesis, Fibres céramiques à base de carbure de silicium et à faible taux d'oxygène, (1995)
[9] R. Bodet, N. Jia, R.E. Tressler, Microstructural Instability and the Resultant Strength of Si-C-O (Nicalon) and Si-N-C-O (HPZ) Fibers, *J. Am. Ceram. Soc.*, **16**, 653-664 (1996).
[10] P. Kroll, Modelling and simulation of amorphous silicon oxycarbide, *J. Mater. Chem.*, **13**, 1657-1668 (2003).
[11] P. Kroll, Modeling the free carbon phase in amorphous silicon oxycarbide, *Journal of Non-Crystalline Solids*, **35**, 1121-26 (2005).
[12] P. Scardi, M. Leoni, R. Delhez, Line broadening analysis using integral breadth methods: a critical review, *Journal of applied crystallography*, **37**, 381-90, (2004)
[13] Th.H. Keijser, E.J. Mittemeijer, H.C.F. Rozendaal, The determination of crystallite-size and lattice-strain parameters in conjunction with the profile refinement method for the determination of crystal structures, *Journal of Applied Crystallography*, **16**, 309-16, (1983)
[14] S. M. Dong, G. Chollon, C. Labrugère, M. Lahaye, A. Guette, J. L. Bruneel, M. Couzi, R. Naslain, D. L. Jiang, Characterization of nearly stoichiometric SiC ceramic fibres, *Journal of Materials Science*, **36**, p. 2371-81 (2001)

[15] J. W. Johnson, D. G. Holloway, On the shape and size of the fracture zones on glass fracture surfaces, *Philosophical Magazine*, **14**, p. 731-43 (1966)
[16] J. J. Mecholsky, S. W. Freiman, R. W. Rice, Fractographic analysis of ceramics, *American Society for Testing and Materials*, p. 363-79, (1978)
[17] L. C. Sawyer, M. Jamieson, D. Brikowski, M. H. Haider, R. T. Chen, Strength, structure, and fracture properties of ceramic fibers produced from polymeric precursors: I, base-line studies, *Journal of the American Ceramic Society*, **70**, 11, p. 798-810 (1987)
[18] I. J. Davies, T. Ishikawa, Estimation of the fracture toughness of Tyranno Si-Ti-C-O fibres from flaw size and "fracture mirror" data measured in situ a 3-D woven SiC/SiC composite, *International Journal of Materials and Product Technology*, **16**, p. 189-96 (2001)
[19] K. Morishita, S. Ochiai, H. Okuda, T. Inchikawa, M. Sato, Fracture toughness of a crystalline silicon carbide fiber (Tyranno-SA3®), *Journal of the American Ceramic Society*, **89**, 8, p. 2571-76 (2006)
[20] A. J. Eckel, R. C. Bradt, Strength distribution of reinforcing fibers in a Nicalon fiber/chemically vapor infiltrated silicon carbide matrix composites, *Journal of the American Ceramic Society*, **72**, 3, p. 455-58 (1989)
[21] B. J. Norman, A. C. Jaras, J. Ashall, Measurement of silicon carbide fibre strength in composites from studies of their fracture surfaces, British Ceramic Transactions, **92**, 2, p. 62-66 (1993)
[22] I. J. Davies, T. Ishikawa, M. Shibuya, T. Hirokawa, Fibre strength parameters measured in situ for ceramic matrix composites tested at elevated temperature in vacuum and air, *Composites Science and Technology*, **59**, 6, p. 801-11 (1999)
[23] M. D. Thouless, O. Sbaizero, L. S. Sigl, A. G. Evans, Effect of interface mechanical properties on pullout in a SiC-fiber-reinforced lithium aluminium silicate glass-ceramic, *Journal of the American Ceramic Society*, **72**, **4**, p. 525-32 (1989)
[24] S. T. Taylor, Y. T. Zhu, W. R. Blumenthal, M. G. Stout, D. P. Butt, T. C. Lowe, New perspective on the fracture of Nicalon fibers, *Fatigue and Fracture Mechanics*, **29**, p. 1-11 (1998)
[25] G. E. Youngblood, C. Lewinsohn, R. H. Jones, A. Kohyama, Tensile strength and fracture surface characterization of Hi-Nicalon SiC fibers, *Journal of Nuclear Materials*, **289**, p. 1-9 (2001)
[26] J. Hurst, H.-M. Yun, D. Gorican, *Advances in ceramic-matrix composites III, Editors N. P. Bansal, J. P. Singh*, CT 74, p. 3 (1996)
[27] W. C. Levengood, Effect of origin flaw characteristics on glass strength, *Journal of Applied Physics*, **29**, p. 820-27 (1958)
[28] L. C. Sawyer, R. Arons, F. Haimbach, M. Jaffe, K. D. Rappaport, Characterization on Nicalon: strength, structure, and fractography, *Ceramic Engineering and Surface Proceedings*, **6**, 7-8, p.567-75 (1985)